


Original Article

CDrift: An Algorithm to Correct Linear Drift From A Single High-Resolution STEM Image

Guillermo Bárcena-González^{1*} , María de la Paz Guerrero-Lebrero¹, Elisa Guerrero¹, Andres Yañez¹, Bernardo Nuñez-Moraleda¹, Daniel Fernández-Reyes², Pedro Real³, David González² and Pedro L. Galindo¹

¹Department of Computer Science and Engineering, University of Cádiz, Puerto Real, Cádiz, Spain; ²Department of Material Science and Metallurgy Engineering and Inorganic Chemistry, University of Cádiz, Puerto Real, Cádiz, Spain and ³Department of Applied Mathematics I, University of Seville, Seville, Spain

Abstract

In this work, a new method to determine and correct the linear drift for any crystalline orientation in a single-column-resolved high-resolution scanning transmission electron microscopy (HR-STEM) image, which is based on angle measurements in the Fourier space, is presented. This proposal supposes a generalization and the improvement of a previous work that needs the presence of two symmetrical planes in the crystalline orientation to be applicable. Now, a mathematical derivation of the drift effect on two families of asymmetric planes in the reciprocal space is inferred. However, though it was not possible to find an analytical solution for all conditions, a simple formula was derived to calculate the drift effect that is exact for three specific rotation angles. Taking this into account, an iterative algorithm based on successive rotation/drift correction steps is devised to remove drift distortions in HR-STEM images. The procedure has been evaluated using a simulated micrograph of a monoclinic material in an orientation where all the reciprocal lattice vectors are different. The algorithm only needs four iterations to resolve a 15° drift angle in the image.

Key words: drift correction, Fourier analysis, image distortion

(Received 6 April 2020; revised 5 June 2020; accepted 19 June 2020)

Introduction

The development of the high-angle annular dark-field (HAADF) technique in scanning transmission electron microscopy (STEM) that provides incoherent imaging without a wave-phase contribution has become increasingly important, because it offers intuitive images whose intensities can be easily interpreted in terms of chemical composition. In particular, the high-resolution (HR)-HAADF imaging technique, which allows the study of crystalline structures at the atomic column scale, helps to clarify the distribution of different elements in crystalline materials (Pennycook & Jesson, 1991). Moreover, the analysis of atomic displacements in HR-HAADF images of a perfect crystal permits the recording of strain maps that reveal the stress state of the nanostructure. However, the scanning can provide incorrect images if the sample holder has a drift during acquisition. This may introduce distortions, expansions, compressions, and shears of the lattice positions that strongly affect such analyses (Nakanishi et al., 2002; Rečnik et al., 2005; Braidy et al., 2012). Despite efforts in STEM microscopes to decrease vibration, air flow/fields, and temperature fluctuations, the presence of sample drift in the captured images is sometimes unavoidable (Von Harrach, 1995; Muller & Grazul, 2001; Sang & LeBeau, 2014).

*Author for correspondence: Guillermo Bárcena-González, E-mail: guillermo.barcelona@uca.es

Cite this article: Bárcena-González G, Guerrero-Lebrero MP, Guerrero E, Yañez A, Nuñez-Moraleda B, Fernández-Reyes D, Real P, González D, Galindo PL (2020) CDrift: An Algorithm to Correct Linear Drift From A Single High-Resolution STEM Image. *Microsc Microanal* 26, 913–920. doi:10.1017/S1431927620001774

For some time now, a number of authors have tried to detect and correct the drift effect in crystalline materials with several approaches, assuming that the images have uniform (Saito et al., 2009; Sang & LeBeau, 2014; Bárcena-González et al., 2018) or non-constant (Berkels et al., 2012a; Sang et al., 2017; Ning et al., 2018; Berkels & Liebscher, 2019) drift rates. Most of them use real-space solutions needing a defect-free zone of reference in the image such as Rečnik et al. (2005), Jones & Nellist (2013), and Zuo et al. (2014). Another major group focuses on the correction of drift in a series of frames from the same region, such as the works proposed by Saito et al. (2009), Berkels et al. (2012b), Binev et al. (2012), Sang & LeBeau (2014), Ophus et al. (2016), Bárcena-González et al. (2016, 2017), or Berkels & Liebscher (2019).

Very recently, we have proposed a simple methodology to correct the lineal drift based on angle measurements between Fourier harmonics in the reciprocal space using a single STEM image (Bárcena-González et al., 2018). However, this approximation is only applicable if the selected orientation has two sets of equivalent planes from the crystallographic point of view—two lattice vectors in the reciprocal space with the same modulus—providing quasi-exact solutions (error below 1%) for drifts lower than 5°. Although, these conditions of the methodology make it applicable for a large number of crystalline materials (cubic and hexagonal in almost all orientations) and usual values of drift (<3°), this approach was not valid for every crystalline orientation in any crystalline system or for large drifts.

In this work, the original formulation using a single STEM image has been extended to be applied to any pair of reciprocal lattice vectors. First, a mathematical formulation describing how

drift and rotation affect the positions of reciprocal lattice vectors in Fourier space is presented, establishing its limits and possible errors. Next, a novel iterative algorithm for correcting drift effect, CDrift, is proposed based on the angle measurements between two reciprocal lattice vectors in Fourier space. Finally, the accuracy of this proposal has been tested in an HR-HAADF-simulated image of a material that does not have two symmetrical reciprocal lattice vectors in any orientation, such as Pu, a monoclinic material with all the reciprocal lattice vectors of unequal modulus. We will show that, even for high drift rates, the CDrift algorithm is able to detect and correct this effect providing very accurate results.

Mathematical Derivation of the Linear Drift Effect

Let us consider a hypothetically drift-free crystal oriented on a pole where atoms have a columnar projection. The lattice positions in the real plane may be defined by two vectors, $\mathbf{a} = (a_x, a_y)$ and $\mathbf{b} = (b_x, b_y)$. The reciprocal lattice vectors associated with green and blue planes are defined by \mathbf{a} and \mathbf{b} as shown in Figure 1, where d_a is the interplanar distance calculated as the distance from point (b_x, b_y) to the line defined by \mathbf{a} ($a_yx - a_xy = 0$), being therefore equal to $d_a = (|a_xb_y - a_yb_x|)/(\sqrt{a_x^2 + a_y^2})$. The reciprocal vector associated with blue planes, \mathbf{a}^* , is perpendicular to \mathbf{a} and has a magnitude equal to $2\pi/d_a$.

$$\mathbf{a}^* = \frac{2\pi}{\|\mathbf{a}\| \cdot d_a} (a_y, -a_x) = \frac{2\pi}{|a_xb_y - a_yb_x|} (a_y, -a_x). \quad (1)$$

The same reasoning may be applied to calculate the reciprocal vector associated with green planes, $\mathbf{b}^* = ((2\pi)/(|a_xb_y - a_yb_x|)) (b_y, -b_x)$, perpendicular to \mathbf{b} and with a module of $2\pi/d_b$. Now, let us state \mathbf{c}_1^* and \mathbf{c}_2^* as the difference between these vectors (see Fig. 2b).

$$\mathbf{c}_1^* = \mathbf{a}^* - \mathbf{b}^* = \frac{2\pi}{|a_xb_y - a_yb_x|} (a_y - b_y, -a_x + b_x), \quad (2)$$

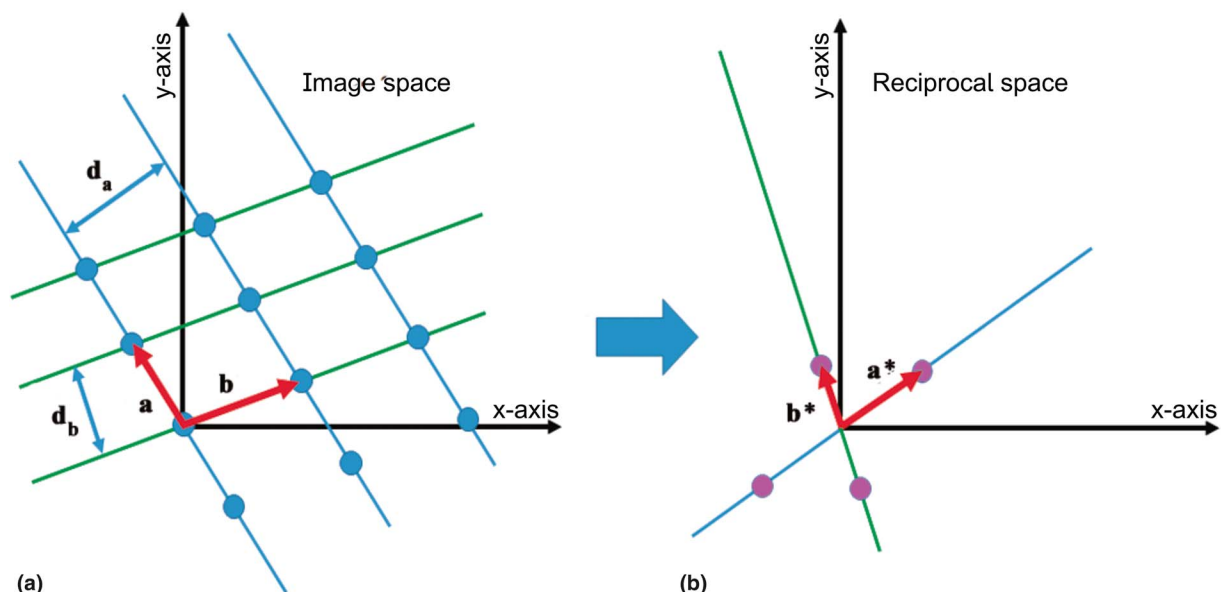


Fig. 1. (a) Image space representing the real lattice defined by basis vectors (\mathbf{a} and \mathbf{b}) and the distances between planes (d_a and d_b) used to geometrically derive the reciprocal vectors \mathbf{a}^* and \mathbf{b}^* for blue and green planes, respectively. (b) Reciprocal lattice vectors (\mathbf{a}^* and \mathbf{b}^*) associated with the lattice described by the basis vectors (\mathbf{a} and \mathbf{b}).

$$\mathbf{c}_2^* = -\mathbf{a}^* - \mathbf{b}^* = \frac{2\pi}{|a_xb_y - a_yb_x|} (-a_y - b_y, a_x + b_x). \quad (3)$$

Let us consider now γ_1 and γ_2 to be the angles between vectors \mathbf{c}_1^* and \mathbf{c}_2^* and the horizontal axis, respectively (see Fig. 2b), numerically calculated using the standard $\text{atan2}(y,x)$ function that returns the four-quadrant inverse tangent of a point (x,y) in the plane. So, γ_1 and γ_2 can be related to the real-space lattice coordinates as:

$$\begin{aligned} \gamma_1 &= \text{atan2}\left(\frac{-a_x + b_x}{|a_xb_y - a_yb_x|}, \frac{a_y - b_y}{|a_xb_y - a_yb_x|}\right) \\ &= \text{atan2}(-a_x + b_x, a_y - b_y), \end{aligned} \quad (4)$$

$$\begin{aligned} \gamma_2 &= \text{atan2}\left(\frac{a_x + b_x}{|a_xb_y - a_yb_x|}, \frac{-a_y - b_y}{|a_xb_y - a_yb_x|}\right) \\ &= \text{atan2}(a_x + b_x, -a_y - b_y). \end{aligned} \quad (5)$$

This is an important modification with respect to our previous paper (Bárcena-González et al., 2018), where only those orientations having two symmetric reciprocal lattice vectors were taken into account. In that case, $\gamma_1 + \gamma_2$ was restricted to be an integer multiple of 90° .

The absolute positions of the reciprocal lattice vectors in this orientation, which define the particular values for γ_1 and γ_2 , are taken as references for the measurement of the so-called rotation angle, ϕ , as 0. However, the sample could generally be rotated counter-clockwise regarding the reference at an angle ϕ when it is introduced into the microscope. Now, we have a new pair of rotated vectors in real space \mathbf{a}' and \mathbf{b}' that mathematically could be described by the corresponding rotation matrix [see equations (6) and (7)]. In the same way, \mathbf{a}^* , \mathbf{b}^* , \mathbf{c}_1^* , and \mathbf{c}_2^* are transformed into \mathbf{a}'^* , \mathbf{b}'^* , $\mathbf{c}_1'^*$, and $\mathbf{c}_2'^*$, respectively. Remarkably, γ_1 and γ_2 angles could be obtained by adding the rotation

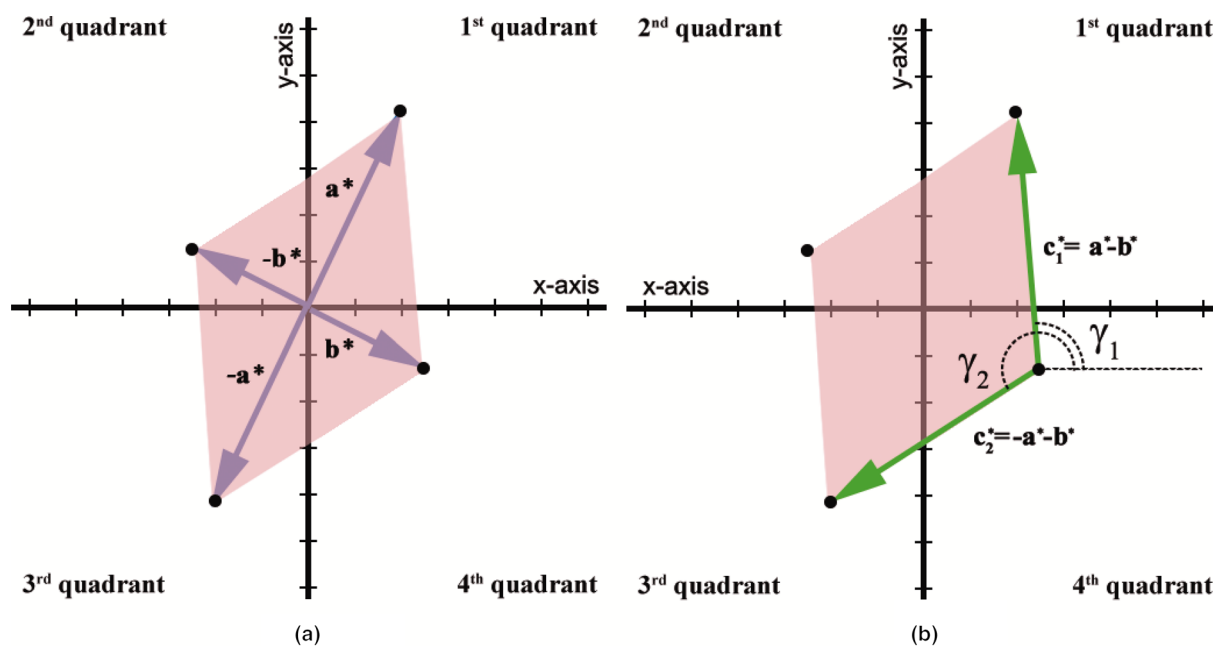


Fig. 2. (a) Reciprocal lattice vectors of a hypothetically drift-free crystal. (b) In green, vectors of differences, \mathbf{c}_1^* and \mathbf{c}_2^* , that form the angles γ_1 and γ_2 with respect to the horizontal axis.

angle ϕ to γ_1 and γ_2 angles, respectively (see Figs. 3a, 3b).

$$\mathbf{a}' = \begin{pmatrix} \cos \phi & \text{amp}; & -\sin \phi \\ \sin \phi & \text{amp}; & \cos \phi \end{pmatrix} \times (a_x, a_y), \quad (6)$$

$$\mathbf{b}' = \begin{pmatrix} \cos \phi & \text{amp}; & -\sin \phi \\ \sin \phi & \text{amp}; & \cos \phi \end{pmatrix} \times (b_x, b_y). \quad (7)$$

Let us consider now how a linear drift affects the positions of the reciprocal lattice vectors in rotated Fourier space. Throughout this work, we will assume that the drift rate is constant along the x-axis of the image in the real space, so the scanning produces a cumulative displacement regarding the y-axis that could be described by a drift angle, α [see Bárcena-González et al. (2018)]. Therefore, this drift also yields a displacement of the lattice vectors in the reciprocal space with respect to the vertical axis,

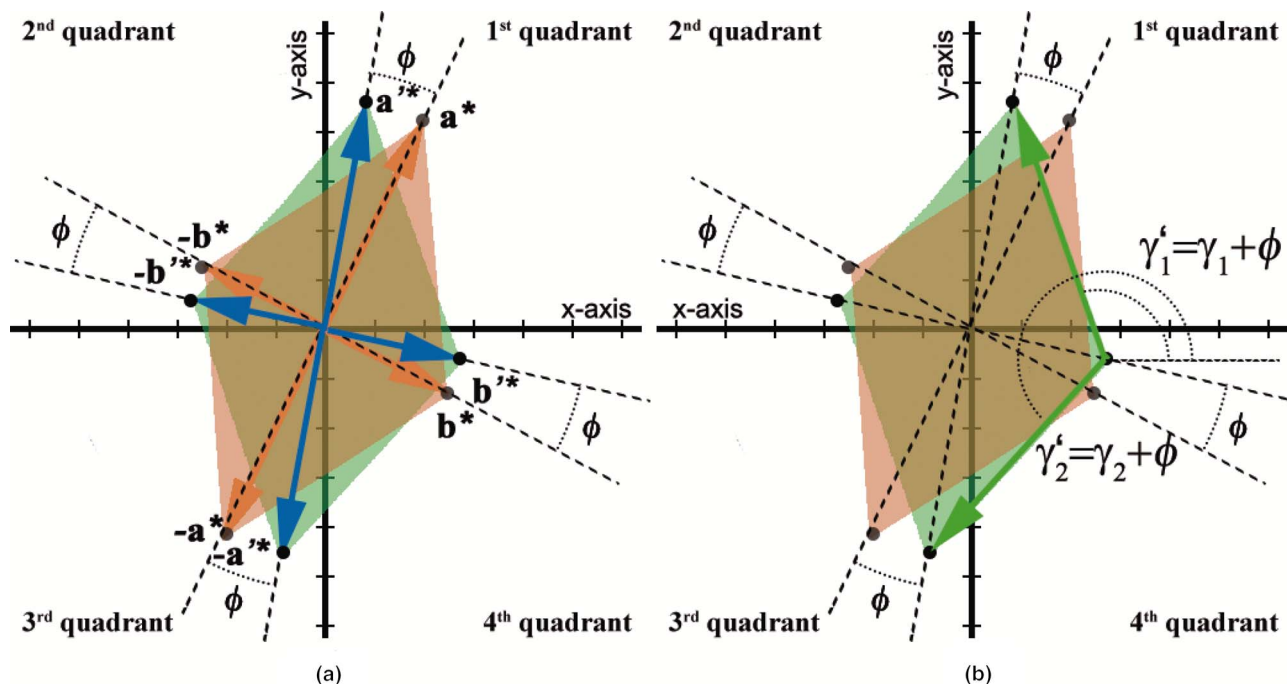


Fig. 3. (a) Image of the hypothetical material rotated an angle ϕ regarding the reference ($\phi=0$). The lattice vectors, \mathbf{a}^* and \mathbf{b}^* , have been marked with orange arrows. In blue, the rotated vectors \mathbf{a}' and \mathbf{b}' . (b) The difference vectors \mathbf{c}_1^* and the corresponding angles γ_1 will be increased by ϕ .

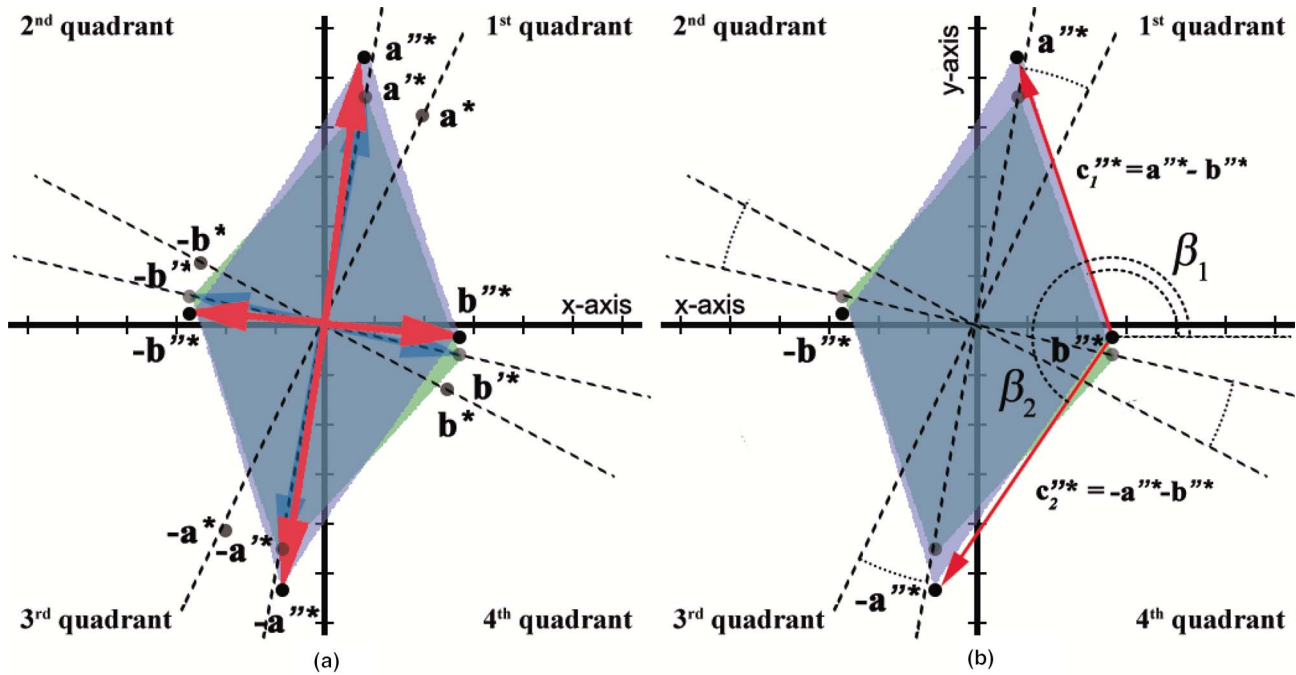


Fig. 4. (a) Displaced peak positions due to the drift effect in the reciprocal space \mathbf{a}^* and \mathbf{b}^* . (b) Vectors \mathbf{c}_1^* and \mathbf{c}_2^* and the angles formed with respect to the horizontal axis β_1 and β_2 .

proportional to the y -component of the vectors and the tangent of the drift angle (α) in real space, generating \mathbf{a}^* and \mathbf{b}^* vectors (see Fig. 4a). Again, we can define two new vectors, \mathbf{c}_1^* as the difference between \mathbf{a}^* and \mathbf{b}^* located between fourth and first quadrants; and \mathbf{c}_2^* , as the difference between $-\mathbf{a}^*$ and \mathbf{b}^* , located between fourth and third quadrants (see Fig. 4b).

Let us denote β_1 and β_2 as the angles of \mathbf{c}_1^* and \mathbf{c}_2^* with respect to the horizontal axis. Both angles, β_1 and β_2 , are the input data obtained from experimental measurements in the reciprocal space in an experimental image with a drift effect. The analytical solution for both angles from the previous formulation is:

$$\beta_1 = \text{atan2}\left(\sigma_2 * \left(\frac{-(a_x - b_x)}{\cos(\alpha)}\right) + \sigma_1 * \left(\frac{-(a_y - b_y)}{\cos(\alpha)}\right), (a_y - b_y) * \cos(\phi) + (a_x - b_x) * \sin(\phi)\right), \quad (8)$$

$$\beta_2 = \text{atan2}\left(\sigma_2 * \left(\frac{(a_x + b_x)}{\cos(\alpha)}\right) + \sigma_1 * \left(\frac{(a_y + b_y)}{\cos(\alpha)}\right), (-a_y - b_y) * \cos(\phi) + (-a_x - b_x) * \sin(\phi)\right), \quad (9)$$

Where

$$\sigma_1 = \sin(\alpha - \phi), \quad (10)$$

$$\sigma_2 = \cos(\alpha - \phi). \quad (11)$$

Some mathematical packages have tried to generate a symbolic solution for α without success. Nevertheless, this mathematical derivation could help us to find certain conditions in which the

equation is simpler and where the drift can be calculated in a precise way. Previously, we demonstrated in Bárcena-González et al. (2018) that the sum of β_1 and β_2 could almost provide us a good approximation of the drift angle under certain conditions (\mathbf{c}_1^* and \mathbf{c}_2^* are perpendicular), with some limitations (drift angles below 5°). In this work, we suggest that the sum between $(\beta_1 - \gamma_1)$ and $(\beta_2 - \gamma_2)$ might allow us to estimate the drift using whatever material without any restriction in the election of the reference reciprocal lattice vectors. Furthermore, any possible rotation ϕ is taken into account using γ_1 , so a coarse value of α could be obtained as follows:

$$\alpha' \approx \beta_1 + \beta_2 - \gamma_1 - \gamma_2 = \beta_1 + \beta_2 - \gamma_1 - \gamma_2 - 2\phi, \quad (12)$$

where β_i are the angle measurements in the experimental image, and γ_i are the ones in the reference drift-free image.

At this point, we can calculate how the drift angle (α) and the rotation angle (ϕ) affect the position of the spots assuming a pair of reciprocal lattice vectors, \mathbf{a}^* located in the first or third quadrant and \mathbf{b}^* located in the second or fourth quadrant. First, for a chosen orientation ($\phi = 0$), γ_1 and γ_2 are constant values that are obtained from equations (4) and (5). Then, α [equation (12)] could be calculated when β_1 and β_2 values are known according to equations (8) and (9). Figure 5 shows the error in degrees as the difference between real drift, α , and the calculated drift, α' , versus the rotation angle (ϕ) for different drift angle values (α). As we can observe, the error is very small for drift angles below 5° at any rotation angle but increases exponentially for higher drift values, especially for rotation angles that are around multiples of $\pi/4$. Regardless, the approach always provides three exact solutions for each drift value. Two of them are the same for all the cases, when $\phi = 0$ or $\phi = \pi/2$, while the third one depends on the α -value, as $\pi/4 - \alpha/2$. The last solution is not useful, as the unknown α is part of the solution. Therefore, if the drift is

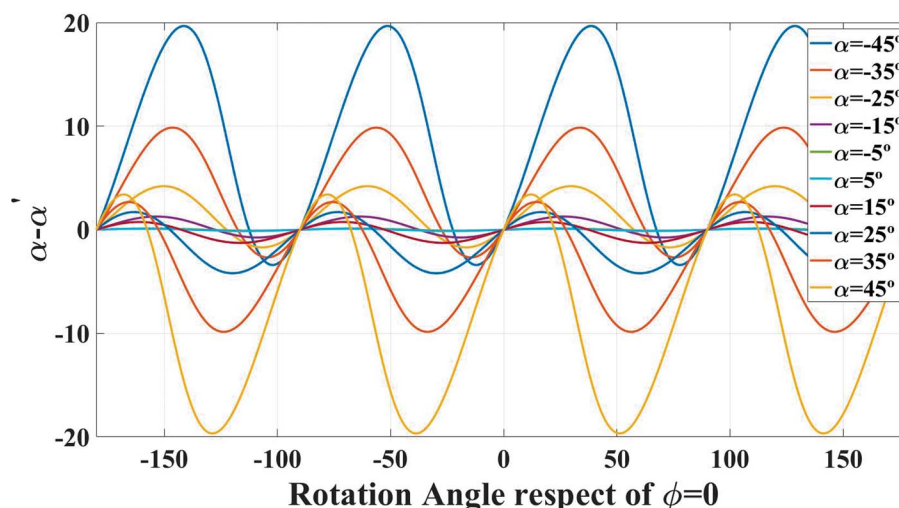


Fig. 5. Error in degrees as the difference between real drift, α , and the calculated drift, α' using equation (12). There exists three algebraic solutions in $0, \pi/2$, and $\pi/4 - \alpha/2$ and multiples of $\pi/2$ of the same values.

parallel or perpendicular to the y -axis in the image, the approach has no error. As we have deduced, the drift could be calculated exactly using equation (12) only for values of ϕ , 0 , or $\pi/2$. However, as the first step consists of rotating the image in such a way that the drift is aligned along the x -axis, ϕ can take any value regarding the reference orientation ($\phi = 0$), which determines the possible values of γ_i .

Materials and Methods

Considering everything, we have developed an iterative algorithm to correct an image affected by a linear drift through a series of steps. The upper limit is imposed by the resolution and the pixel density of the image, that is, the algorithm will iterate until the increase/decrease of the measured drift (α) in the successive iterations, does not produce an image deformation of at least one pixel ($\Delta\alpha$). The code for determining the drift angle of an experimental image (CDrift) is explained in the following and given at the end of this section. First, we must enter the coordinates of the reference lattice positions in the reciprocal space of a perfect crystal ($\mathbf{a}^*, \mathbf{b}^*$) for a defined orientation, $\phi = 0$, which are constant for this pole and may be calculated from crystallographic tables in the case of a well-known material and also from another drift-free image in the same orientation. To increase the precision of the angle measurement, it is recommended to use the position of the second harmonic or beyond, as described in Bárcena-González et al. (2018). Next, in the real image, which is probably rotated regarding the reference coordinates at an angle ϕ , the coordinates of two selected reciprocal lattice positions ($\mathbf{a}_i^*, \mathbf{b}_i^*$) have to be determined. Then, the algorithm works by iteratively finding the rotation angle, ϕ . For this, the image is rotated up to the x -component of the selected spots is as close as possible to the x -component of the reference. The precision of the calculation is defined by $\Delta\phi$ giving the first approximation to ϕ . In the rotated image, β_1 and β_2 could be analytically calculated using equations (8–11). Now, it is possible to draw the first α'_1 by applying equation (12) and use it to correct the image. This process is repeated until the correction of α is null, which directly depends on the pixel resolution of the original image ($\Delta\alpha$).

Algorithm CDrift($\mathbf{a}^*, \mathbf{b}^*$)
$\mathbf{c}_1^* \leftarrow \mathbf{a}^* - \mathbf{b}^* \quad \mathbf{c}_2^* \leftarrow -\mathbf{a}^* - \mathbf{b}^*$
$\gamma_1 \leftarrow \text{atan2}(\mathbf{c}_{1y}^*, \mathbf{c}_{1x}^*) \quad \gamma_2 \leftarrow \text{atan2}(\mathbf{c}_{2y}^*, \mathbf{c}_{2x}^*)$
$X_0 \leftarrow \{\mathbf{a}_x^*, \mathbf{b}_x^*, -\mathbf{a}_x^*, -\mathbf{b}_x^*\} \quad Y_0 \leftarrow \{\mathbf{a}_y^*, \mathbf{b}_y^*, -\mathbf{a}_y^*, -\mathbf{b}_y^*\}$
while $\alpha' \leq \Delta\alpha$
Pick in the image the spots of the fundamental frequencies
$X_d \leftarrow \{\mathbf{a}_{ix}^*, \mathbf{b}_{ix}^*, -\mathbf{a}_{ix}^*, -\mathbf{b}_{ix}^*\}$
$Y_d \leftarrow \{\mathbf{a}_{iy}^*, \mathbf{b}_{iy}^*, -\mathbf{a}_{iy}^*, -\mathbf{b}_{iy}^*\}$
Calculate the position of the harmonics
$\phi \leftarrow 0$
Do
$\text{aux} \leftarrow \cos(\phi) * X_0 - \sin(\phi) * Y_0$
$\phi \leftarrow \phi + \Delta\phi$
while $\sum \sqrt{(\text{aux} - X_d)^2} \cong 0$
$Z_1 \leftarrow \{X_{d1} - X_{d3}, Y_{d1} - Y_{d3}\} \quad Z_2 \leftarrow \{X_{d3} - X_{d2}, Y_{d3} - Y_{d2}\}$
$\beta_1 \leftarrow \text{atan2}(Z_{1y}, Z_{1x}) \quad \beta_2 \leftarrow \text{atan2}(Z_{2y}, Z_{2x})$
$\gamma'_1 \leftarrow \gamma_1 - \phi \quad \gamma'_2 \leftarrow \gamma_2 - \phi$
$\alpha' \leftarrow \beta_1 + \beta_2 - \gamma'_1 - \gamma'_2 - 2\phi$
end-while
return ϕ, α'

Application of CDrift

To show the accuracy and robustness of CDrift as well as its feasibility for any orientation and crystallography, the proposed methodology has been applied to an HR HAADF-STEM-simulated image of a Pu crystal along the [010] direction. The lattice parameters of the unit cell of Pu are $a = 6.183, b = 4.822, c = 10.963 \text{ \AA}$; $\beta = 101.79^\circ$ (Zachariasen & Ellinger, 1963). We have used this monoclinic material because in that orientation all of the reciprocal lattice vectors have different magnitudes. A Pu drift-free image ($1,536 \times 1,536$ pixels with a resolution of

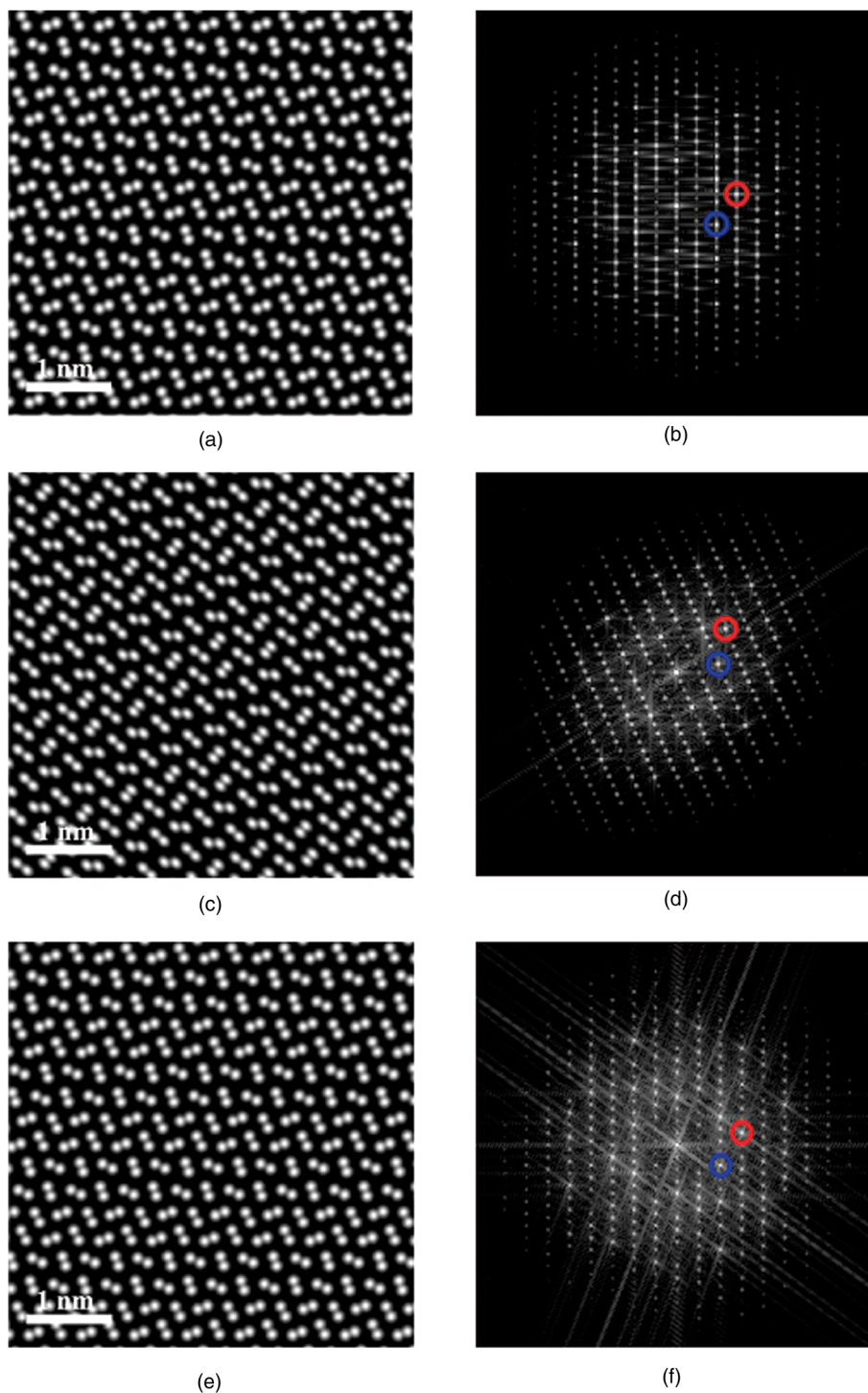


Fig. 6. (a) Simulated image of a perfect crystal of Pu along [010]. The y direction of the image corresponds to [001]. That is the reference orientation, $\phi = 0$. (b) FFT of this perfect crystal. The coordinates of the selected spots (circles in red and blue) are the first inputs to CDrift. (c) Image of Pu with a rotation of 21.63° and distorted with a drift angle of 15°. (d) FFT of the previous image and the corresponding spots. (e and f) Final image after applying CDrift and the corresponding FFT, respectively.

185 pixels per nanometer) was simulated along [010], with the following conditions: a 100 kV-dedicated VG Microscope HB501UX STEM, $C_s = -50 \mu\text{m}$, $C_5 = 63 \text{ mm}$, inner detector angle = 70 mrad, outer detector angle = 200 mrad, and objective aperture = 27 mrad (Fig. 6a). The chosen reference orientation ($\phi = 0$) is that in which the y direction of the image corresponds to the [100] direction of the unit cell. Figure 6b displays the fast

Fourier transform (FFT) of this perfect crystal in this reference orientation. The first inputs to the CDrift procedure are the coordinates of the selected spots in Figure 6b (X_o , Y_o) that allow calculating the corresponding γ_i . These coordinates, which correspond to two sets of planes, are constants that could be obtained from the crystallographic tables of the material (Chateigner et al., 2020).

Table 1. Iterations Of CDrift In Order To Calculate α and ϕ Angles.

	Iteration 1	Iteration 2	Iteration 3	Iteration 4	Sum
α	13.007°	2.037°	0.167°	0.015°	15.226°
ϕ	21.606°	21.506°	21.506°	21.506°	

α is calculated as the sum of the values obtained in each iteration and ϕ as the value obtained in the last iteration.

In Figure 6c, the simulated image has been rotated an angle $\phi = 21.63^\circ$ regarding the reference and a drift effect of $\alpha = 15.01^\circ$ included, corresponding to a sample drift of 0.023 nm/s for a pixel dwell time of 40 μ s. The linear drift effect was simulated shifting to the right a pixel every few rows of pixels in each row of the image that is proportional to the distance from the upper left corner of the image. Certainly, the drift profile is not exactly continuous but with discrete changes. However, given the pixel density used (185 pixels/nm), we consider this effect to be

negligible. Figure 6d shows the corresponding FFT of this simulated image that represents the experimental image.

The algorithm starts by asking for the reference lattice vectors in the real space in the reference orientation, then these vectors are used to calculate γ_i values. Next, in order to apply an FFT to the experimental image, the user must select the spots corresponding to the reference vectors. To improve the accuracy of the calculations, it is recommended to use the spots corresponding to the second or higher harmonics. In each iteration, the drift effect α_i is corrected, and the reconstructed image is progressively closer to the drift-free image (see Figs. 6e, 6f). Only four iterations have been needed to obtain a linear drift of 15.226° and a rotation angle of 21.506°, as shown in Table 1.

The errors with respect to the initial values of ϕ and α are 0.124° and 0.216°, respectively. In addition, the reconstructed step-by-step image is better than the one obtained in one step. The algorithm will finish iterating when the value of the drift calculated in that iteration is less than a step value. This value would be the minimum angle that produces any change in the image, that is, the drift that produces at least one pixel shift in the image.

In order to analyze the drift effect as well as the quality of the drift correction, the use of histograms of the distances between neighboring atom-columns gives an accurate picture (Sang & LeBeau, 2014). For this, we define two atomic distances between the bases, as shown in the inset of Figure 7a, and represent the distances obtained for the whole image using histograms. The atom column positions are defined using a normalized cross-correlation approach and Gaussian peak fitting (Zuo et al., 2014). Figure 7 shows the histograms of the drift-free simulated image, the drift-distorted simulated image, and the drift-corrected image. For the case of a perfect image without drift (Fig. 6a), two thin peaks are clearly formed in Figure 7a. In contrast, the atom distance histogram (Fig. 7b) obtained from the image with drift distortion (Fig. 6c) has not maximized distances. Finally, the atom distance histogram in Figure 7c, which corresponds to the drift-corrected image using CDrift, is very similar to that obtained from a perfect crystal. Our methodology has achieved a quasi-perfect correction of large linear drifts (greater than 15°) in a monoclinic crystal where the reciprocal network vectors are all different.

Conclusions

In this paper, we have developed the mathematical derivation of the linear drift effect in an HAADF-STEM image, analyzing how affects the positions of the reciprocal lattice positions in the Fourier space. As there is not a manageable analytical equation to deduce drift angle, we have proposed an iterative algorithm to detect and correct linear drift using a single HAADF-STEM image, CDrift, based on rotation calculations and the measurements of the displaced reciprocal vectors. This method generalizes and outperforms our previous scheme for any crystalline material and orientation.

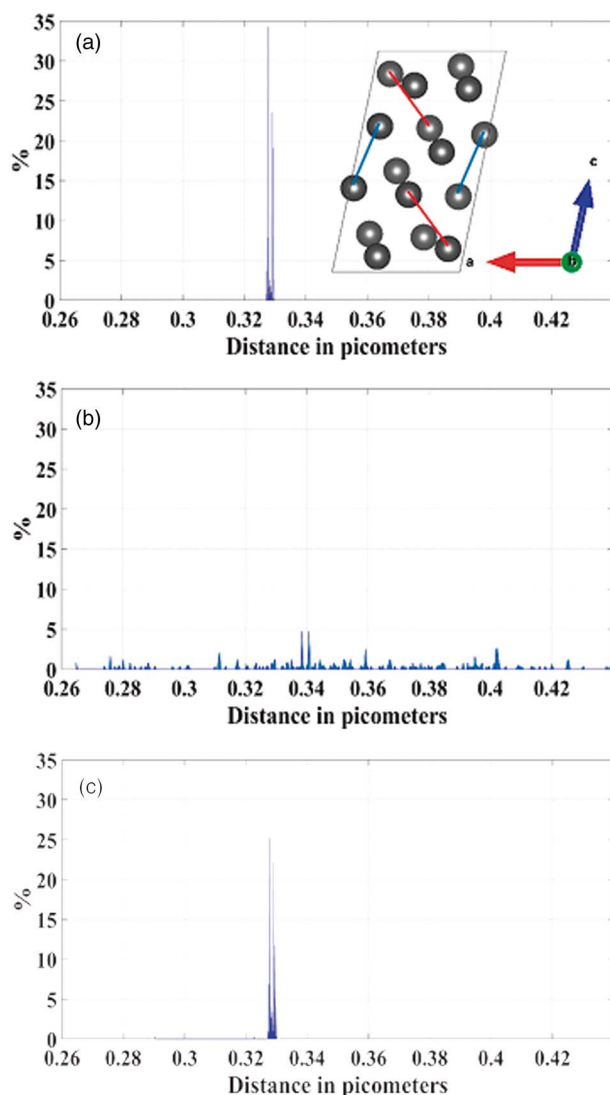


Fig. 7. (a) Distance histogram of the reference image of Figure 6a. The selected distances between the atomic columns are pointed in the inset. Two thin peaks are clearly defined. (b) Atom distance histogram of the drifted image of Figure 6c. The drift distortion deeply flattens the distance histogram. (c) The corresponding atom distance histogram of the reconstructed image of Figure 6e. Atomic distances have less dispersion and are again defined in two peaks in the histogram.

Acknowledgments. We acknowledge funding from the Spanish Government (projects MAT2016-77491-C2-2-R and TEC2017-86102-C2-2-R) and SCCYT-UCA for technical support.

References

- Bárcena-González G, Guerrero-Lebrero MP, Guerrero E, Fernández-Reyes D, González D, Mayoral A, Utrilla JM, Ulloa JM & Galindo PL (2016). Strain mapping accuracy improvement using super-resolution techniques. *J Microsc* **262**(1), 50–58. doi:10.1111/jmi.12341
- Bárcena-González G, Guerrero-Lebrero MP, Guerrero E, Reyes DF, Braza V, Yañez A, Nuñez-Moraleda B, González D & Galindo PL (2018). Correcting sample drift using Fourier harmonics. *Micron* **110**. doi:10.1016/j.micron.2018.04.004
- Bárcena-González G, Guerrero-Lebrero MP, Guerrero E, Yañez A, Fernández-Reyes D, González D & Galindo PL (2017). Evaluation of high-quality image reconstruction techniques applied to high-resolution Z-contrast imaging. *Ultramicroscopy* **182**, 283–291. doi:10.1016/j.ultramic.2017.07.014
- Berkels B & Liebscher CH (2019). Ultramicroscopy Joint non-rigid image registration and reconstruction for quantitative atomic resolution scanning transmission electron microscopy. *Ultramicroscopy* **198**, 49–57. doi:10.1016/j.ultramic.2018.12.016
- Berkels B, Sharpley R, Binev P, Yankovich A, Shi F, Voyles P & Dahmen W (2012a). High precision STEM imaging by non-rigid alignment and averaging of a series of short exposures. *Microsc Microanal* **18**(S2), 300–301.
- Berkels B, Yankovich AB, Shi F, Voyles PM, Dahmen W, Sharpley R & Binev P (2012b). High precision STEM imaging by non-rigid alignment and averaging of a series of short exposures. *Microsc Microanal* **18**(S2), 300–301. doi:10.1017/S1431927612003352
- Binev P, Blanco-Silva F, Blom D, Dahmen W, Lamby P, Sharpley R & Vogt T (2012). High-quality image formation by nonlocal means applied to high-angle annular dark-field scanning transmission electron microscopy (HAADF-STEM). *Nanostruct Sci Technol*. doi:10.1007/978-1-4614-2191-7_5.
- Braidly N, Le Bouar Y, Lazar S & Ricolleau C (2012). Correcting scanning instabilities from images of periodic structures. *Ultramicroscopy* **118**, 67–76. doi:10.1016/j.ultramic.2012.04.001
- Chateigner D, Chen D, Ciriotti D, Downs RT, Gražulis S, Kaminsky W, Le Bail A, Lutterotti L, Matsushita Y, Merkys A, Moeck P, Murray-Rust P, Quirós Olozábal M, Rajan H & Yokochi AFT (2020). Crystallography Open Database. Available at <http://www.crystallography.net/cod/index.php>.
- Jones L & Nellist PD (2013). Identifying and correcting scan noise and drift in the scanning transmission electron microscope. *Microsc Microanal* **19**(4), 1050–1060. doi:10.1017/S1431927613001402
- Muller A & Grazul J (2001). Optimizing the environment for sub-0.2 nm scanning transmission electron microscopy. *J Electron Microsc* **50**(3), 219–226. doi:10.1093/jmicro/50.3.219
- Nakanishi N, Yamazaki T, Rečnik A, Čeh M, Kawasaki M, Watanabe K & Shiojiri M (2002). Retrieval process of high-resolution HAADF-STEM images. *J Electron Microsc* **51**(6), 383–390. doi:10.1093/jmicro/51.6.383
- Ning S, Fujita T, Nie A, Wang Z, Xu X, Chen J, Chen M, Yao S & Zhang T (2018). Scanning distortion correction in STEM images. *Ultramicroscopy* **184**, 274–283. doi:10.1016/j.ultramic.2017.09.003
- Ophus C, Ciston J & Nelson CT (2016). Correcting nonlinear drift distortion of scanning probe and scanning transmission electron microscopies from image pairs with orthogonal scan directions. *Ultramicroscopy* **162**, 1–9. doi:10.1016/j.ultramic.2015.12.002
- Pennycook SJ & Jesson DE (1991). High-resolution Z-contrast imaging of crystals. *Ultramicroscopy* **37**(1–4), 14–38. doi:10.1016/0304-3991(91)90004-P
- Rečnik A, Möbus G & Šturm S (2005). IMAGE-WARP: A real-space restoration method for high-resolution STEM images using quantitative HRTEM analysis. *Ultramicroscopy* **103**(4), 285–301. doi:10.1016/j.ultramic.2005.01.003
- Saito M, Kimoto K, Nagai T, Fukushima S, Akahoshi D, Kuwahara H, Matsui Y & Ishizuka K (2009). Local crystal structure analysis with 10-pm accuracy using scanning transmission electron microscopy. *J Electron Microsc* **58**(3), 131–136. doi:10.1093/jmicro/dfn023
- Sang X & LeBeau JM (2014). Revolving scanning transmission electron microscopy: Correcting sample drift distortion without prior knowledge. *Ultramicroscopy* **138**, 28–35. doi:10.1016/j.ultramic.2013.12.004
- Sang X, Lupini AR, Ding J, Kalinin SV, Jesse S & Unocic RR (2017). Precision controlled atomic resolution scanning transmission electron microscopy using spiral scan pathways. *Sci Rep* **7**, 43585. doi:10.1038/srep43585
- Von Harrach HS (1995). Instrumental factors in high-resolution FEG STEM. *Ultramicroscopy* **58**(1), 1–5. doi:10.1016/0304-3991(94)00172-J
- Zachariasen WH & Ellinger FH (1963). The crystal structure of alpha plutonium metal. *Acta Crystallogr* **16**(8), 777–783. doi:10.1107/S0365110X63002012
- Zuo J-M, Shah AB, Kim H, Meng Y, Gao W & Rouvière J-L (2014). Lattice and strain analysis of atomic resolution Z-contrast images based on template matching. *Ultramicroscopy* **136**, 50–60. doi:10.1016/j.ultramic.2013.07.018